Sustainable Energy & Fuels

ROYAL SOCIETY OF CHEMISTRY

PAPER

View Article Online
View Journal | View Issue

Cite this: *Sustainable Energy Fuels*, 2024, **8**, 2219

A mesoporous Ta_2O_5/Nb_2O_5 nanocomposite with Lewis/Brønsted acid sites to enhance stepwise glucose conversion to 5-hydroxymethylfurfural†

Sangeeta Mahala,[ab] Senthil Murugan Arumugam,[a] Ravi Kumar Kunchala,[a] Bhawana Devi[ab] and Sasikumar Elumalai *[a]

Herein, we report a higher formation of 5-hydroxymethylfurfural (HMF), a potential liquid fuel precursor, using glucose over a bifunctional Ta_2O_5/Nb_2O_5 composite. The mesoporous nanocomposite comprising 25% wt Nb_2O_5 provides both Lewis (24%) and Brønsted acid (76%) sites, with increased oxygen vacancies. The former sites can facilitate glucose isomerization to fructose, while the latter condition promotes fructose dehydration to HMF. Therefore, it enables the systematic conversion of glucose into HMF through the formation of fructose, resulting in 78.6% HMF and 86.5% selectivity after 3 h at 170 °C. The rate kinetics reveals that glucose degradation follows a second-order rate law with a rate constant (k_G) of 2.4×10^{-2} L mol^{-1} s^{-1}. On the other hand, fructose decomposition follows first-order kinetics with a rate constant (k_{Fru}) of 1.3×10^{-3} s^{-1}, but it also leads to significant unwanted side product formation (with a rate constant of $k_2 = 4.7 \times 10^{-5}$ s^{-1}). Both glucose and fructose decompositions to HMF exhibit temperature-dependent kinetics, as indicated by the Arrhenius plots. The calculated reaction thermodynamic parameters of glucose and fructose decomposition to HMF by employing the Eyring–Polanyi theory establish a comparable feasibility $\Delta G°$ of 124.2–132.5 kJ mol^{-1}, with non-spontaneous reaction characteristics ($\Delta S^{\#}$ of −109.0 to −259.6 J mol^{-1} K^{-1}).

Received 15th February 2024
Accepted 3rd April 2024

DOI: 10.1039/d4se00228h

rsc.li/sustainable-energy

Introduction

The energy crisis and environmental constraints, such as growing global energy demands, depleting non-renewable fossil fuels, increasing greenhouse gas emissions, and rising fuel prices, urge the immediate development and use of sustainable and renewable energy fuels.[1] In recent years, intensive research has been undertaken to produce direct liquid fuels (such as ethanol)[2] and their precursor molecules (such as furan derivatives)[3,4] using renewable and abundantly available biomass resources. Among them, furan compounds can be readily obtained from lignocellulosic biomass through chemical conversions, specifically 5-hydroxymethylfurfural (HMF).[5] It has been established as versatile in the preparation of potential fuel additive compounds, such as 2-methylfuran, 2,5-dimethylfuran, *etc.*, owing to its cyclic aldehyde structural characteristics with both aldehyde and alcohol reactive functional groups.[6] Typically, glucose or fructose is used for its production,[7,8] but most studies have focused on glucose utilization because it comprises up to 40% of the lignocellulosic biomass by weight.[4] In this regard, to date, a variety of homogeneous and heterogeneous catalytic setups have been developed and reported to yield 75–80% HMF with >80% selectivity.[9,10] Comparatively, heterogeneous catalytic systems have gained more interest due to the recyclability option, which can significantly reduce the operating cost from a commercial perspective. Moreover, solid materials can enable the fine-tuning of catalytic activities and provide active sites on a wide platform, thereby facilitating selective glucose conversion.[11] Many studies have utilized metal oxides for HMF production due to their abundance and lower cost. However, when using glucose, it typically follows a sequential transformation, *i.e.*, glucose is first isomerized to fructose, followed by dehydration to HMF.[12,13] Moreover, these conversions operate under different conditions, *i.e.*, Lewis acid conditions facilitate glucose isomerization,[14] whereas Brønsted acid conditions favor fructose dehydration.[15] Thus, the studies insist on the provision of varied strength acidic sites by a single catalyst for effective glucose conversion.

In this context, Morales *et al.* developed a mesoporous tantalum oxide (Ta_2O_5) catalyst, an amorphous solid, that can offer a high level of both Lewis and Brønsted acid sites of 353 μmol NH_3 g^{-1} upon its treatment with a non-ionic surfactant (Pluronic L-121).[16] However, this resulted in a moderate HMF

[a]*Chemical Engineering Division, DBT-Center of Innovative and Applied Bioprocessing, Mohali, Punjab 140306, India. E-mail: sasikumar@ciab.res.in; Tel: +91-172-5221-444*
[b]*Department of Chemical Sciences, Indian Institute of Science Education and Research (IISER), Mohali, Punjab 140306, India*

† Electronic supplementary information (ESI) available: Details of materials and methods; catalyst characterization results (BET and TPD-NH_3 desorption); experimental results on product formation (using glucose and fructose); rate kinetic results of glucose and fructose and their thermodynamic parameter values. See DOI: https://doi.org/10.1039/d4se00228h

yield of 23% using glucose through a 69% substrate conversion at 175 °C after 90 min. But it exhibited good stability during recycling by controlling the Ta species leaching under elevated conditions. Additionally, it demonstrated regaining the maximum catalytic activity *via* a routine calcination technique. In another study, niobium pentoxide (Nb_2O_5) was established as promising for converting both monosaccharides and polysaccharides into HMF,[17] attributed to its strong acidic characteristics (*i.e.*, $H_0 \leq -5.6$, which is nearly 70% the strength of H_2SO_4). The hydrated form of Nb_2O_5 could achieve as high as 89% HMF formation using fructose and 54% using inulin at 160 °C in a water-2-butanol biphasic medium. This can be correlated with its active acidic functionality (*i.e.*, 3-fold higher acidic sites than that of the hydrated Ta_2O_5) and surface area.[18] However, these materials could achieve only average productivity. This is mainly caused by the ensuing side reactions under elevated conditions, such as unwanted humin (an unstructured molecule) formation and HMF rehydration to equal amounts of levulinic acid (LA) and formic acid (FA).[17] A higher number of Lewis acid sites with fewer Brønsted sites is ineffective in the dehydration reaction, whereas the reverse combination is harmful to the reaction. Thus, a balanced presence of Lewis and Brønsted acidic sites can enable selective product synthesis through a systematic approach. Therefore, we designed a composite catalyst by blending Nb_2O_5 with Ta_2O_5 to provide a balanced presence of Lewis and Brønsted acid active sites for converting glucose into HMF *via* fructose formation.[18,19] For the development of the solid catalyst, we followed a template-free nonhydrolytic sol–gel method by utilizing mixtures of *n*-butanol and *tert*-butanol as a solvent, along with the $NbCl_5$ and $TaCl_5$ precursors.[20] In this method, *n*-butanol serves as a capping agent, facilitating the formation of metal alkoxides that undergo minimal hydrolysis. Additionally, the growth rate of particles can be regulated. Similarly, *tert*-butanol aids in the formation of multiple metal hydroxide groups through M–O–M bond formation by combining with the available M–Cl species. However, elemental chlorine is generated when primary alcohols engage with MCl_5 for the first time; this allows primary alcohols to undergo a partial reduction of M^{5+} cations to M^{4+} subsequently. Upon release of the chlorine atom, any remaining unreacted alcohols are expected to undergo oxidation under the prevailing conditions, potentially leading to aldehyde and hydrochloric acid formation. This approach allows for developing a mesoporous mixed metal oxide material with improved pore volume and surface area properties, with tuned active Lewis and Brønsted acid sites. As a result, the catalyst exhibits enhanced durability for multiple reuses. We applied chemical reaction engineering principles to gain insights into the kinetics and mechanism of the two-step reactions.[21] The calculated thermodynamic parameters have suggested the feasibility of the reactions of glucose and fructose into HMF.

Experimental

Chemicals and reagents

Chemicals and reagents, including D-glucose, D-fructose, HMF, LA, FA, niobium pentachloride ($NbCl_5$, 99%), tantalum pentachloride ($TaCl_5$, 99.99%) and dimethyl sulphoxide (DMSO) were purchased from Sigma Aldrich (India). Acetic acid, *n*-butanol and *tert*-butanol were purchased from Merk India. Absolute ethanol was purchased from Fisher Scientific India. All these chemicals purchased were of analytical grade and used as received unless otherwise mentioned. Deionized water (DI) obtained from a Millipore water purifier system (Millipore) was used for sample preparation and dilution purposes.

Ta_2O_5/Nb_2O_5 composite preparation

A template-free sol–gel method was followed for the mixed metal oxide catalyst preparation, as reported elsewhere.[22,23] $TaCl_5$ (0.810 g) and $NbCl_5$ (from 0.231 g to 0.540 g) were mixed in a 10.8 mL butanol mixture (equal volumes of *n*-butanol and *tert*-butanol) in a 250 mL beaker. The solid–liquid mixture was stirred vigorously (450 rpm) for 2 h at room temperature. The resultant was then transferred to a Teflon-lined autoclave and aged for 24 h at 160 °C. Followed this, the solid was collected *via* high-speed centrifugation (10 000 rpm) and washed thoroughly using water and ethanol. Thereafter, it was dried under vacuum at 90 °C and labelled as Ta/Nb-1.5 (15% Nb_2O_5). A similar procedure was followed to prepare other combinations of Ta_2O_5/Nb_2O_5, such as Ta/Nb-2.5 (25% Nb_2O_5), and Ta/Nb-3.5 (35% Nb_2O_5), but with a proportional loading of $NbCl_5$. For comparison, pristine metal oxides, namely Ta_2O_5 and Nb_2O_5, were prepared by using just a single precursor. For gaining insights into the surface properties of the catalysts (such as Ta_2O_5, Nb_2O_5 and Ta/Nb-2.5), a part of the as-synthesized materials was calcined at 500 °C for 2 h at a ramp rate of 3 °C per min (ref. 16) and labelled as Ta-cal, Nb-cal and Ta/Nb-2.5 cal, respectively.

Analytical characterization techniques

An X-ray diffractometer instrument (XRD; Rigaku. Smart LAB SE) was used to determine the structure and phase purity of the as-prepared catalysts under a Cu-Kα radiation source. The samples were scanned at $\lambda = 1.541$ from 10° to 80°. The functional group determination was performed using a Fourier transform-infrared spectrometer (FTIR; Agilent Technologies Cary 600 series). The surface morphological examination was performed using a field-emission scanning electron microscope instrument (FE-SEM; Hitachi SU8010). For this, the sample was immobilized on a copper holder coated with platinum containing a conducting resin and was analyzed at 30 mA for 30 s. The elemental fraction determination and mapping analysis were performed using an embedded energy-dispersive X-ray spectroscope instrument (FESEM-EDX; Hitachi SU8010). For gaining more insights into the structural features, a high-resolution transmission electron microscope (JEOL-JEM-2100 Plus) analysis was performed. For the analysis, the sample was prepared by evenly distributing it on a carbon grid. The characterization studies of binding energy and oxidation state of the metal ions in the catalyst were performed using an X-ray photoelectron spectrophotometer equipped with an Al-Kα X-ray source (XPS; PHI 5000 VersaProbe III). The C 1s signal (285.08 eV) was used as a calibration reference for data processing. BET

analysis for determining the surface properties was performed using a Quantachrome Autosorb iQ instrument. The total pore volume was determined under 0.99 relative pressure (P/P_0) of N_2. The Barrett–Joyner–Halenda (BJH) and multipoint BET methods were used to calculate the average pore width and pore size distribution. Prior to analysis, the sample was degassed for 8 h at 100 °C under a N_2 gas stream. The acidic site measurement was performed *via* temperature-programmed desorption of ammonia by using an NH_3-TPD BELCAT II instrument equipped with a TCD detector. For the analysis, a quartz tube containing 55 mg catalyst was heated for 60 min at 200–400 °C under a 50 mL min^{-1} He gas stream. After this, the material was cooled down to 50 °C, and the amount of NH_3 desorption was measured under continuous gas flow conditions (50 mL min^{-1}). The experiment was conducted at a ramp rate of 10 °C min^{-1} starting from 50 °C up to 750 °C. The *in situ* diffusion Fourier transform infrared spectroscopy (DRIFT) analysis was performed using a Bruker VERTEX 70 FTIR spectrometer equipped with a mercury cadmium telluride (MCT) detector. Before analysis, the sample was pretreated under N_2 flow conditions at 300 °C for 60 min and cooled down to room temperature. Following this, it was placed under a He balanced NH_3 gas stream to adsorb NH_3 gas on the catalyst surface at 30 °C for 60 min. It was then purged by flushing the N_2 gas to remove the residual NH_3 content. After all, the spectral measurement was performed at 30 °C. The desorption study of the adsorbed NH_3 was performed up to 250 °C to determine the stability of the Lewis and Brønsted acidic sites at higher temperatures.

Catalytic synthesis of HMF using monosaccharides

In a typical catalytic HMF reaction, 20 mg glucose/fructose was dissolved in 5 mL DI water or binary solvent (water–DMSO) in a 35 mL glass reactor (Ace glass, Sigma Aldrich). Different ratios of catalyst to substrate load were used, corresponding to 15%, 25% and 50% wt. The batch reactor was then tightly sealed, shaken slightly and placed in a pre-heated hot oil bath of 160–190 °C. The reaction was conducted under vigorous stirring conditions (500 rpm). After a 5 h reaction (maximum), the reactor was quenched in an ice bath. The contents of the reactor were collected and centrifuged at high speed (10 000 rpm) to separate the solid and liquid portions. From the liquid portion, an aliquot was collected, diluted and analyzed on a high-performance liquid chromatography (HPLC) device equipped with a refractive index (RI) detector, which was maintained at 55 °C. An Agilent Hi-Plex H column (300 mm length and 8 μm porosity) was used for the sample analysis, which was maintained at 65 °C. A 5 mM dilute H_2SO_4 solution was used as a mobile phase at 0.7 mL min^{-1} flow. The product(s) and residual sugar concentrations were determined using the calibration standard obtained using the respective standard chemicals. The product yield and selectivity, and substrate conversion calculations were performed using the mathematical expressions presented in the ESI (eqn (S1)–(S3)†). Alongside this, the recovered catalyst was washed thoroughly with water and ethanol, dried under vacuum overnight and stored for recycling purposes. A similar sugar dehydration protocol was followed to determine the catalyst's recyclability. All experiments were conducted in duplicate. The data are an average of two runs. The statistical analysis was performed using the SPSS software by employing the two-way ANOVA method. All graphical results were obtained using the OriginPro software (OriginLab, USA).

Results and discussion

Physico-chemical characterization of the catalyst

Pristine and composite metal oxides, either with or without calcination, were characterized by employing various analytical techniques. In the X-ray diffraction pattern (Fig. 1a), broad and less intense bands can be observed, indicating the amorphous nature of the catalysts. However, calcination transformed the amorphous characteristics into crystalline structures, particularly with Nb. This transformation is evident from the peaks observed at 22.5°, 28.5°, 36.7°, 46.1°, 50.5°, and 55.1°, which correspond to the (001), (100), (101), (002), (110), and (102) diffraction planes,[24] respectively (Fig. S1a†). On the other hand, Ta maintained its amorphous nature even under high-temperature calcination, as indicated by the broad peaks at 25.8°, 34.2°, and 55°.[16] Crystalline Nb_2O_5 was found to be in the TT-Nb_2O_5 format, as per PDF card no. 00-028-0317,[23] due to the calcination at 500 °C.[25] In contrast, all composites (namely Ta/Nb-1.5, Ta/Nb-2.5, and Ta/Nb-3.5) exhibited a similar XRD pattern to pristine Ta_2O_5, with peaks at 25.6° and 55.4°, confirming their amorphous properties. In the case of Ta/Nb-2.5 and Ta/Nb-3.5, the presence of more Ta_2O_5 is apparent from a new peak observed at 33.6°. Catalysts with higher content of Nb_2O_5, such as Ta/Nb-1.5, displayed dominant characteristics of Nb_2O_5. This is evident from the absence of a peak related to Ta_2O_5 in Ta/Nb-1.5. Conversely, Ta/Nb-2.5-cal showed several new peaks at 22.9°, 28.4°, 36.9°, 46.9°, 50.5°, and 55.9°, corresponding to the (001), (100), (101), (002), (110), and (102) planes, respectively, confirming the presence of multiple crystal phases (the phases are most likely orthorhombic (β-Ta_2O_5) and tetragonal (α-Ta_2O_5), belonging to Ta_2O_5). Thus, low-temperature calcination (500 °C) did not affect the amorphous nature of the material. However, >700 °C can cause a phase change to either the orthorhombic (β-Ta_2O_5) or tetragonal (α-Ta_2O_5) structure depending on the low or high annealing temperature of Ta_2O_5 and a transformation into a crystalline structure.[26] In contrast, Nb-cal exhibited a notable peak at 55°, which can be attributed to Nb_2O_5, confirming its crystalline pseudo-hexagonal TT-phase.[23] This transition from an amorphous to a slightly anisotropic state is possible at higher annealing temperatures. When comparing the results, the composites showed slight peak shifts compared to the pristine ones, indicating probable interactions between the metal species. In the FTIR spectrum of composites (Fig. 1b), the broad absorption peaks that emerge between 3400 cm^{-1} and 1615 cm^{-1} correspond to the asymmetric and symmetric stretching vibrations of the hydroxyls (–OH) belonging to the absorbed water molecules and the surface hydroxyls.[16,23] The prominent peaks at 430.80–436.62 cm^{-1}, 487.9–492.12 cm^{-1}, and 565.32–567.89 cm^{-1} correspond to the metal–oxygen stretching frequencies. Similarly, the peaks in the 487.90–492.12 cm^{-1} region correspond

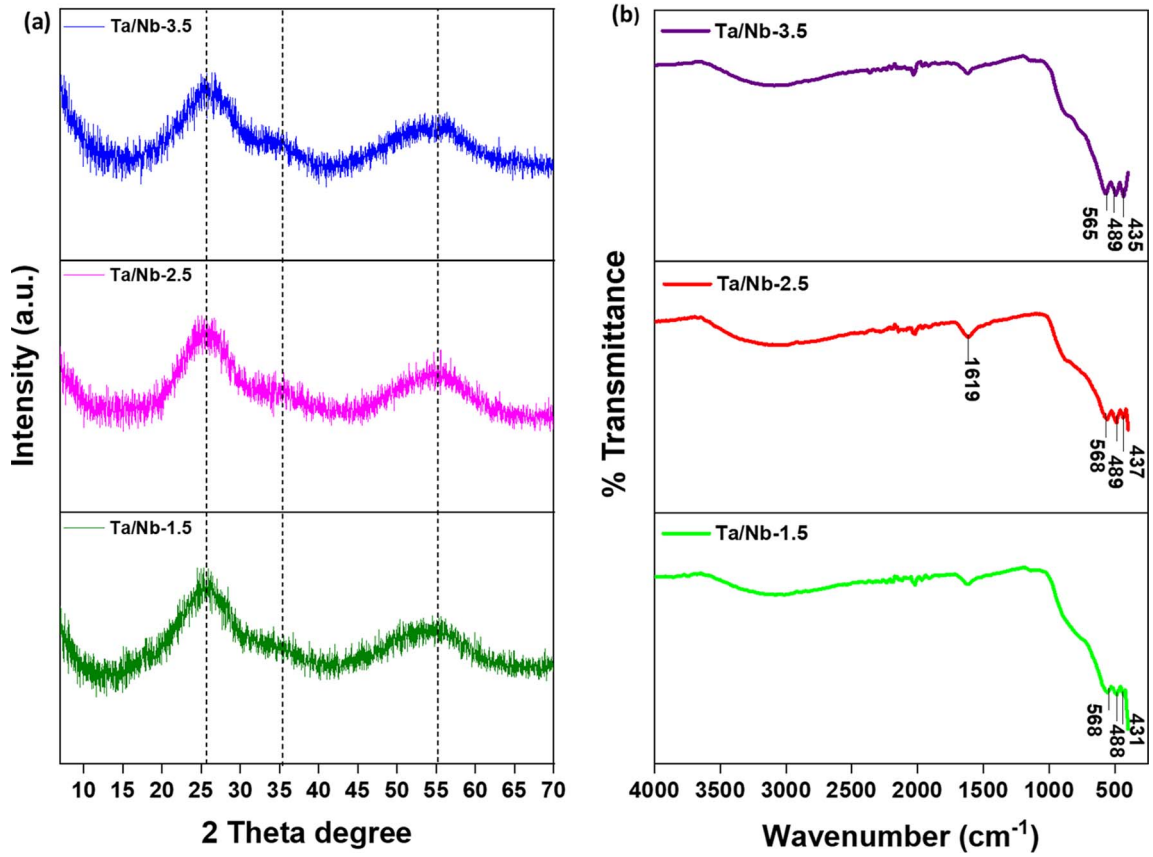

Fig. 1 (a) XRD patterns and (b) FTIR spectra of the as-synthesized Ta/Nb composites.

to M = O (where, M is Nb/Ta) stretching frequencies, establishing the formation of M_2O_5.[13] The metal oxide interactions in the individual catalysts can be verified from the peaks at 567.89 cm^{-1} (Ta/Nb-1.5), 567.89 cm^{-1} (Ta/Nb-2.5) and 565.32 cm^{-1} (Ta/Nb-3.5) corresponding to the bridging M–O–M.[27] When comparing the results of composites, absorption peaks had a slight shift, suggesting the interaction of Nb_2O_5 with Ta_2O_5. As Nb precursor content increases, the absorption peaks shift towards a higher wavenumber, demonstrating the higher strength of the bond. But in the Ta/Nb-1.5 combination, this effect was observed to be similar to that of Ta/Nb-2.5, describing the excess Nb precursor not interacting with Ta_2O_5 and being available in a free state.

It can be observed that the catalysts exhibit the corresponding characteristics of the dominant metal oxide. The higher thermal stability of the composite catalysts can be confirmed from the TGA characterization, as shown by the results in Fig. S1b.† Up to 200 °C, the catalysts exhibited a normal weight loss of up to 12.4%, caused by surface water evaporation, with the composition having a minimal impact. Beyond this temperature, the catalysts experienced a gradual weight loss of up to 9% (cumulative) throughout the entire temperature range (up to 800 °C). This is likely caused by the decomposition of organic substances inside the mesopores of the sample and the phase transition of the material at higher temperatures.[28] The residual capping agents (such as *n*-butanol and *tert*-butanol) can undergo oxidation under the prevailing conditions to form aldehydes and hydrochloric acid. At higher temperatures, the evaporation of these moieties can lead to an increased weight loss of the catalyst particle. But the trace moieties may not play a role in the catalytic activity.[16] Among the composites, Ta/Nb-3.5 exhibited the lowest weight loss of 18.3% (cumulative), which is approximately 15% lower than that of the others. This indicates higher thermal stability of Ta_2O_5 and less phase transition compared to Nb_2O_5. We intentionally skipped the TGA characterization of pristine Ta_2O_5 and Nb_2O_5, as they are extensively investigated.[16,25] As per the XRD characterization, Nb_2O_5 is more sensitive to annealing temperatures; therefore its higher content in the composites, namely Ta/Nb-2.5 and Ta/Nb-1.5, can enable the phase transition, resulting in weight loss.

By employing XPS characterization, it is possible to observe how the electronic structure and oxidation state of the catalysts (Ta_2O_5 and Nb_2O_5) are altered upon mixing and the relation between their catalytic activity. Fig. S2† displays the survey spectrum of the catalysts. In the spectrum, Nb_2O_5 shows two distinct peaks centered at binding energies of 206.98 eV and 209.68 eV (Fig. 2a), which correspond to the Nb $3d_{5/2}$ and Nb $3d_{3/2}$ states, respectively. An energy separation of 2.70 eV indicates the presence of the Nb^{5+} state.[29,30] Conversely, pristine Ta_2O_5 exhibits asymmetric peaks with a binding energy separation of 1.9 eV between Ta $4f_{7/2}$ (26.10 eV) and Ta $4f_{5/2}$ (27.98 eV). From this, it can be inferred that Ta attains complete oxidation to reach its Ta(v) state.[31,32] Anticipating the result, Ta/Nb-2.5 exhibits a merged characterization but with a shift in

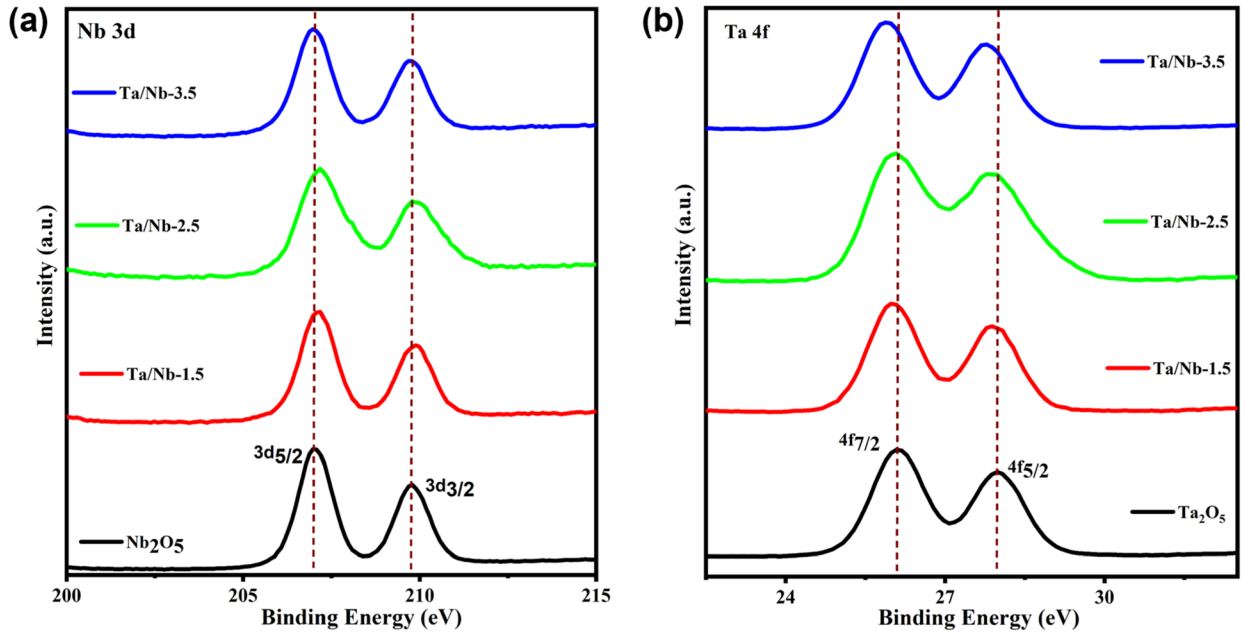

Fig. 2 Comparative deconvolution results of (a) Nb 3d and (b) Ta 4f peaks of the as-synthesized pristine and composite catalysts.

binding energy. The shift is towards increased binding energy, particularly in the Nb 3d peaks, compared to those of pristine Nb_2O_5. This shift can be attributed to an electronic interaction difference between the two phases of Ta_2O_5 and Nb_2O_5,[33] arising from varying chemical interactions or chemical bonding between the phases (Fig. 2a) due to the slightly different cationic sizes of Nb^{5+} (having a 3d orbital) and Ta^{5+} (having both 3d and 4f orbitals).[34] As per the atomic arrangement (from left to right), Nb^{5+} (4d series) has a slightly smaller atomic radius when compared to Ta^{5+} (5d series). Therefore, the Nb^{5+} cation may have a higher electronegativity compared to Ta^{5+} and undergo a strong interaction with oxygen, leading to an increase in the binding energy, particularly in the Nb 3d peaks, compared to pristine Nb_2O_5. This can be evident from the shift towards increased binding energy, resulting in a shorter bond compared to that of Ta_2O_5. This leads to the creation of more oxygen vacancies in the composite and facilitates a strong interfacial contact between Ta_2O_5 and Nb_2O_5, causing a binding energy difference in Ta 4f. As a consequence, the shift is towards lower binding energy compared to that of pristine Ta_2O_5 (Fig. 2b). By analyzing the O 1s XPS data, it is possible to explain the interaction of Ta–O and Nb–O. The binding energies of O 1s in the

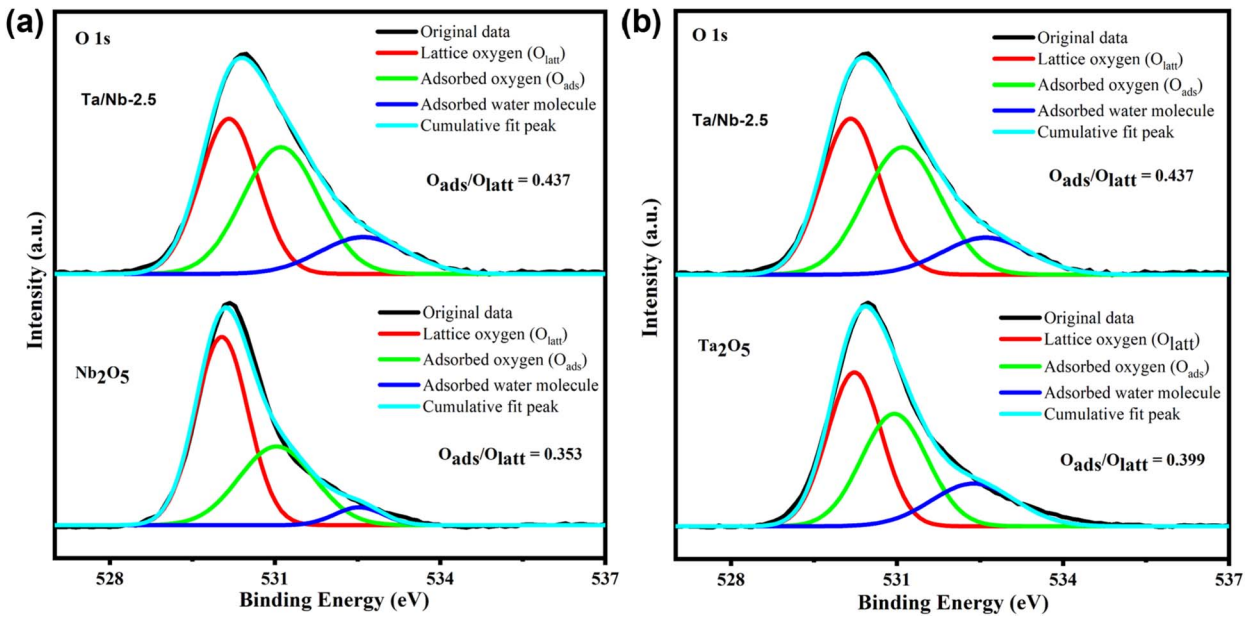

Fig. 3 Comparative deconvolution results of the O 1s peak in pristine (a) Nb_2O_5 and (b) Ta_2O_5 and Ta/Nb-2.5 catalysts.

Ta/Nb composite showed changes compared to those of the pristine ones (Fig. 3a and b).

These changes are attributed to the presence of oxygen vacancy defects, which enable the interfacial contact between the two phases of the composites and result in a binding energy shift. Upon deconvolution of the O 1s spectrum, three peaks corresponding to lattice oxygen (O_{latt}), surface adsorbed oxygen (O_{ads}), and adsorbed water molecules are observed within a binding energy range of 529.2–530 eV, 531.2–532 eV, and 532.3–532.9 eV, respectively (Fig. 3a and b).[35,36] A similar peak pattern was observed in other composites, such as Ta/Nb-1.5 and Ta/Nb-3.5 (Fig. S3a and b†), confirming their catalytic characteristics. Among them, Ta/Nb-2.5 exhibited the highest amount of adsorbed oxygen, indicating a larger number of oxygen vacancies. This feature can play a vital role in catalytic reactions by enhancing the interaction between the catalyst and reactant through absorption and desorption processes.[37]

The porosity of the catalysts was determined *via* N_2 physisorption analysis (Fig. S4a†). All catalysts exhibited a type IV hysteresis loop within the relative pressure range of 0.1–1.0, as classified by the IUPAC.[17,18,23] The calculation of the BJH pore size distribution revealed a broader pore size distribution for the solid. Evidently, there are significant differences in surface area, pore volume, and pore size values between the calcined and uncalcined materials. The deviation in the calcined material is likely due to pore blockage under higher temperature conditions and the transformation from an amorphous into a crystalline structure. In Table 1, the differences in surface area, total pore volume, and pore size of Ta-cal can be seen as nominal when compared to those of Ta_2O_5 (without calcination), but they are significant compared to those of Nb_2O_5. Pristine Nb_2O_5 is represented as a microporous material based on the pore diameters measuring 0.47 nm and 1.68 nm for calcined and uncalcined solids, respectively. Similarly, Ta_2O_5 was estimated to have a pore diameter of 3.14 nm, with a mesoporous structure before calcination, but the calcination affected the pore diameter to 1.22 nm (microporous). This is likely caused by shrinkage of pores at high temperatures and increased crystallinity. Thus, the composites with pore diameters between 2.59 nm and 2.87 nm can be classified as mesoporous structures. According to reports, materials with higher surface area and porosity are beneficial for catalytic reactions. Hence, the uncalcined composite was chosen for the glucose dehydration reaction instead of the calcined ones. Regarding the surface area, the as-synthesized composites were investigated in the range of 142–178 $m^2\ g^{-1}$, which is significantly higher than that of pristine metal oxides. Among these, Nb_2O_5's contribution is more pronounced, as indicated by the results of composites with varied ratios of Nb_2O_5. In other words, the lower the Nb_2O_5 content, the smaller the particle surface area, and *vice versa*. Based on these findings, the composite's architecture can be imagined in such a way that Nb_2O_5 occupies the pores of Ta_2O_5 and make interaction to some extent and, beyond that, forms a permanent deposition on the latter's surface. This deposition may occur in the interstitial spaces between the crystallites. Moreover, the pores exhibited random sizes and shapes, likely due to the effect of template-free particle synthesis, highlighting the importance of a template for obtaining uniform particle size. Therefore, the increased surface area is likely a result of the obstruction of the catalyst's pores by the surface-deposited solid. This can be confirmed by the results of the calcined composite (Ta/Nb-2.5 cal), which exhibited microporous characteristics with decreased surface area and pore diameter, supporting the selection of uncalcined composites for catalysis. The acidic characteristics were determined *via* TPD analysis (Fig. S4b†), which revealed that the surface acidity is increased due to the individual metal ions (Nb^{5+} and Ta^{5+}). According to the literature, this acidity is influential in the catalytic conversion of glucose into HMF *via* dehydration.[16–18] However, the acidic strength depends on the oxidation capacity and vacant d-orbitals. The total acidic strength of the catalysts was determined through NH_3-TPD analysis. Comparative results show that the catalysts exhibit similar characteristics at all tested temperatures, ranging from 50 °C to 700 °C, regardless of their varying elemental composition. It can be presumed that the pretreatment temperatures maintained during TPD and DRIFT analyses are not high enough to induce phase changes in the metal oxides. For instance, Ta_2O_5 exhibited an amorphous nature up to 500 °C, with negligible changes in surface area before and after calcination, based on the XRD findings. But significant changes were observed in pristine Nb_2O_5 at 500 °C. As per the reports, Nb_2O_5 can exhibit an amorphous structure up to 400 °C, with no phase changes.[38] Notably, the intervention of Nb_2O_5 is minimal. Moreover, Nb^{5+} increases the total acidic sites of the catalysts. But beyond a Ta/Nb ratio of 2.5, the catalysts experience a slight decrease in the acidic strength (Table 1), caused by a higher Nb content, which can affect the interaction of metal oxides and increase the inactive surface area. The observed acidic sites were weak to moderate, which is favorable for glucose dehydration *via* fructose intermediate formation. As previously reported, Ta_2O_5 and Nb_2O_5 catalysts offer either Lewis or Brønsted acidity, resulting in a 50–60% HMF yield through glucose isomerization and fructose dehydration steps.[16,17] Therefore, the as-synthesized composites offering both weak and moderate acidity can further improve the yield when using glucose.

Table 1 Results of physisorption and chemisorption analyses of the catalysts

Surface characteristics	Nb	Nb-Cal	Ta	Ta-Cal	Ta/Nb-1.5	Ta/Nb-2.5	Ta/Nb-3.5	Ta/Nb-2.5-Cal
Surface area ($m^2\ g^{-1}$)	73.650	8.901	38.335	36.400	178.070	143.510	142.172	99.110
Total pore volume ($cm^3\ g^{-1}$)	0.045	0.104	0.030	0.023	0.116	0.103	0.094	0.084
Average pore diameter (nm)	1.687	0.469	3.142	1.229	2.591	2.870	2.651	1.687
Acidic sites (mmol g^{-1})	0.258	0.223	0.335	0.168	0.641	0.665	0.616	0.466

As per the literature, $Nb_2O_5 \cdot nH_2O$ and $Ta_2O_5 \cdot nH_2O$ can exhibit both terminal and bridging hydroxyls; therefore, they can offer both Lewis and Brønsted acid sites on their surface.[17,39] Specifically, the Lewis acid sites are characterized by electron-deficient centers that can accept electrons through their empty orbitals. Hypothetically, strong Lewis acid sites can originate from the low coordinated M-O_4 and M-O_5 in $Nb_2O_5 \cdot nH_2O$ and $Ta_2O_5 \cdot nH_2O$, whereas the weak Lewis acidity comes from the highly distorted M-O_6.[40] A typical NH_3 adsorption study was performed to determine the type of acidic sites *via* DRIFT analysis. After successful NH_3 adsorption, the effect of temperature on the Lewis and Brønsted sites was evaluated by recording the *in situ* temperature-resolved DRIFT spectra of NH_3 desorption. The spectra displayed two peaks in all catalysts, with a slight peak shift (Fig. 4a–e), particularly with the peaks at 1608 cm^{-1} (δAS(N–H)) and 1234 cm^{-1} (δS(N–H)), which are attributed to the asymmetric and symmetrically coordinated NH_3 bound to Lewis acid sites, respectively.[41,42] Two additional peaks at 1662 cm^{-1} (δS(N–H)) and 1420 cm^{-1} (δAS(N–H)) can be assigned to the symmetric and asymmetric ionic NH_4^+ bound to Brønsted acid sites. However, Ta_2O_5 did not show any symmetric ionic NH_4^+ bound at 1662 cm^{-1} (Fig. 4a). In Ta_2O_5, the quantity of Lewis (47.33%) and Brønsted (52.68%) acidic sites was found to be almost equal, based on the peak area; therefore, it may have a higher impact only on the first step (glucose isomerization). On the other hand, Nb_2O_5, estimated to have a higher percentage of Brønsted sites (73.10%) and a lower percentage of Lewis sites (26.90%), can be influential for the second step (fructose dehydration) and, to some extent, the first step as well.

Based on this, the composites (Ta/Nb-1.5 and Ta/Nb-2.5), having nearly 75.8% Brønsted sites with 24.2% Lewis sites on average, can be expected to be effective in promoting conversions. However, these composites exhibited a similar ratio of acidic sites, indicating the saturation of the interaction between Ta_2O_5 and Nb_2O_5. A further decrease in Nb_2O_5 content has altered the pattern, resulting in 39.4% Lewis acid sites and 60.5% Brønsted acid sites, likely due to the dominant characteristics of Ta_2O_5 in the composite. Thus, an excessive amount of Nb_2O_5 cannot provide a synergistic effect with Ta_2O_5. Furthermore, it may remain in a free state, leading to an increase in the catalyst's inactive surface area, as observed in the BET analysis (Fig. S4a†). While studying the effect of temperature on the stability of the acidic sites, it was observed that the intensity of all the bands, including NH_4^+ coordinated with Brønsted acid sites (at 1662.52 cm^{-1} and 1420.10 cm^{-1}) and NH_3 coordinated with Lewis acid sites (at around 1608.23 and 1234.12 cm^{-1}), was slightly affected by temperature (Fig. S4b†). At temperatures >150 °C, a significant decrease in the intensity of Brønsted acid sites was observed, indicating the relatively weaker thermal stability of NH_3 species interacting with the Brønsted acid sites compared to those adsorbed on Lewis acid sites. Thus, the results indicate that blending Nb_2O_5 with Ta_2O_5 can alter the strength of the acidic sites, improving the essential Brønsted acid sites for sugar catalysis, especially fructose dehydration to HMF.

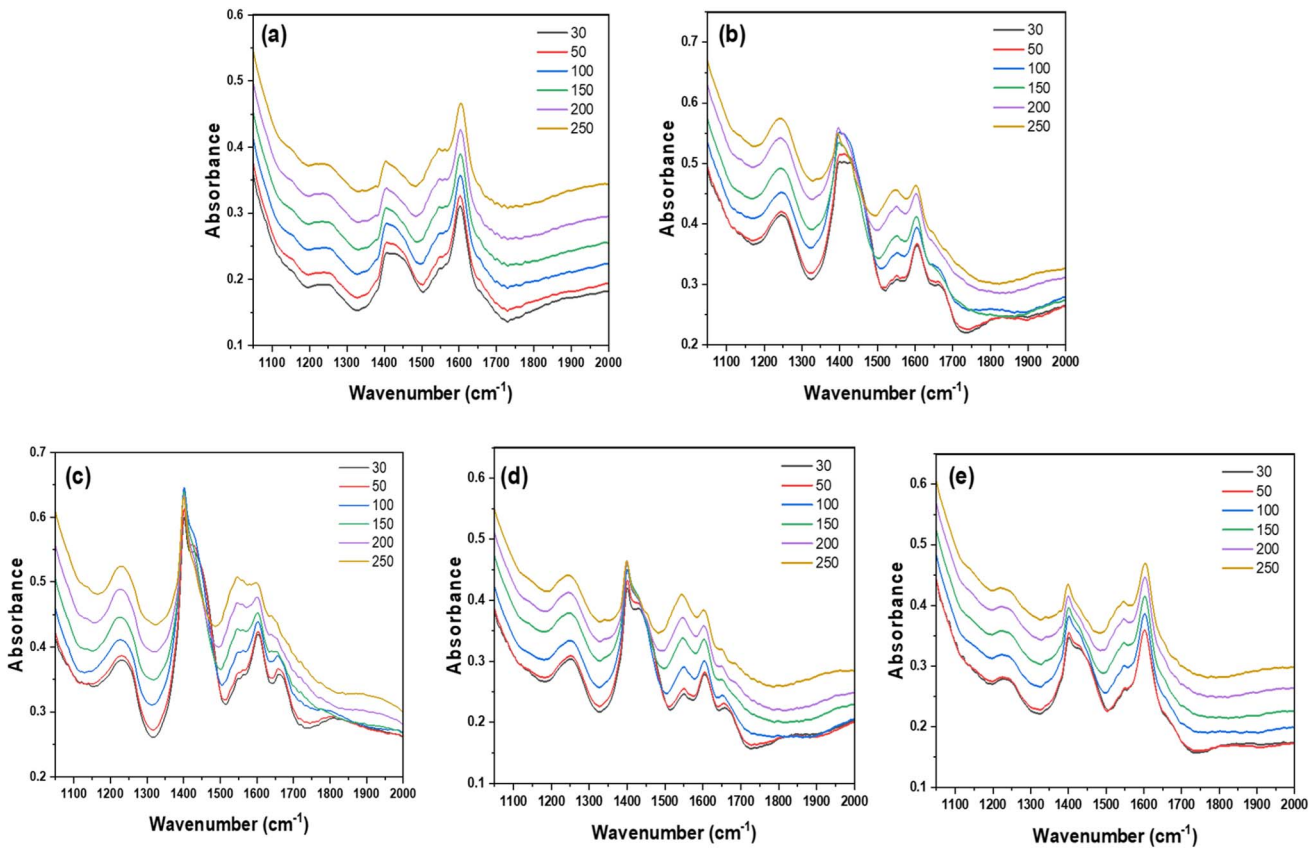

Fig. 4 *In situ* temperature-resolved DRIFT spectra of NH_3 desorption over (a) Ta_2O_5, (b) Nb_2O_5, (c) Ta/Nb-1.5, (d) Ta/Nb-2.5 and (e) Ta/Nb-3.5.

The SEM analysis of Ta/Nb-2.5 verified the particle agglomeration during synthesis, consequently yielding particles of irregular shapes measuring in the 4–20 nm range (Fig. S5a and b†).[43] The FE-SEM and EDX mapping results validate its chemical composition, *i.e.*, 16.7% Nb, 37.5% Ta, and 45.7% O atoms (consistent with the initial supply), as well as its purity (Fig. S6†). Furthermore, the images display the widespread distribution of the individual metal oxides in the composite. The TEM analysis revealed the characteristics of the amorphous material (Ta/Nb-2.5) as having no specific morphology and particle size (Fig. S5c and d†). Thus, the comprehensive analytical characterization studies confirm the structural organization of the composite catalyst, where Nb_2O_5 is deposited on the surface of Ta_2O_5. The outer particles can provide Lewis and Brønsted acidic sites over a wide surface area, which is favorable for glucose isomerization and dehydration, resulting in enriched HMF formation. Additionally, the metal oxides present as Ta^{5+} and Nb^{5+} can be beneficial for ionic interactions with sugar molecules to influence degradation. The composite, with its mesopores, is an added advantage as it can accommodate more sugar molecules for the reaction.

Catalytic activity of the Ta_2O_5/Nb_2O_5 nanocomposite in glucose conversion to HMF

Thus, the analytical techniques confirmed the structural configuration of the as-synthesized catalyst(s) which could offer both the crucial Lewis/Brønsted active sites over the wide surface area, which are favorable for the glucose dehydration to HMF. The catalyst screening process began with pristine, calcined, and uncalcined metal oxides under elevated conditions, specifically at 170 °C for up to 4 h in a water medium. The pristine Ta_2O_5 and Nb_2O_5 catalysts demonstrated the ability to synthesize HMF, but only at a yield of 11–13%. Unfortunately, a significant amount of fructose remained unreacted in the medium, ranging from 13–15%. This indicates that the conditions were not conducive to enabling a stepwise conversion. Ta_2O_5, which offers a high percentage of Lewis acidic sites (47.3%), was effective in glucose isomerization, resulting in the production of 15% fructose. On the other hand, Nb_2O_5, which provides a higher percentage of Brønsted sites (73.1%), promoted HMF formation, resulting in 5 times more HMF compared to Ta_2O_5 (Fig. S7 and Table S1†). However, an excess of Brønsted acidic sites can lead to multiple side reactions,[17] resulting in a higher glucose conversion rate of 50%. The results obtained from the calcined catalysts showed that the acidic sites affect not only productivity but also the surface properties, specifically surface area and porosity. For example, the calcined pristine metal oxides exhibited a reduced surface area (up to 8-fold) and pore diameter (3–4-fold), leading to a 1–5 times reduction in HMF formation with a proportional amount of residual fructose. When evaluating the effectiveness of the composites, it was found that all of them improved productivity, yielding 21.8% HMF and 41.4% selectivity, but with an average residual fructose concentration of 13.9%. However, they exhibited varying catalytic activity depending on their physicochemical characteristics. For example, the Ta/Nb-1.5 catalyst, represents a 1 : 1.5 wt ratio of Nb_2O_5 to Ta_2O_5 and exhibits dominant characteristics of Nb_2O_5, especially a Brønsted acidity of 75.7%, and has achieved 21.6% HMF and 3.7% selectivity, but at the expense of a glucose conversion of 61.1%. Similarly, the catalyst with the lowest ratio of Nb_2O_5 resulted in poor HMF productivity with a yield of 11.0% and 20.3% selectivity. According to Fig. S7,† the optimum blending of Nb_2O_5 with Ta_2O_5 to achieve a maximum yield of 21.8% HMF and 41.4% selectivity is at a 1 : 2.5 wt ratio. Furthermore, the results of Ta/Nb-2.5 cal reinforced the speculation that surface characteristics are crucial for the conversion process. It is evident that the conditions influenced HMF degradation (Fig. S8†), which is possible in a water medium, resulting in up to 10.7% LA formation, regardless of the acidic strengths (Table S2†).

Therefore, catalysis was performed in a binary solvent system (4 : 1 vol. ratio of DMSO to water), where the catalysts' performance was found to be remarkable, yielding relatively 3.5-fold higher HMF while maintaining a similar productivity trend as in a water medium (Fig. 5a). Among all composites, Ta/Nb-2.5 showed promise, achieving a high HMF yield of 78.6% and selectivity of 86.5% with a turnover number (TON) of 0.033 s^{-1} (Table S3†). However, the rehydration of HMF to LA and FA proved uncontrollable under the prevailing conditions, mainly due to the presence of 1/4th of a volume of water. This reduced selectivity and complicated downstream product recovery. Notwithstanding this, the conditions led to other undesired glucose degradations, including humin formation,[44] resulting in an approximately 15% sugar loss that couldn't be accounted for (Table S4†). Nevertheless, this is a common phenomenon in sugar conversion under elevated conditions and cannot be avoided entirely.[45] However, the system has recovered considerable fructose as unconverted, affecting the maximum HMF formation. Nonetheless, the result is comparable to the literature reports (70% HMF on average).[9,10,46] On a positive note, this affirms the ability of the bifunctional catalyst to enable a cascade glucose conversion through fructose intermediate formation, attributed to the presence of a significant number of Lewis acid sites (~24%). Thus, the results verify the consistency with the postulation that the fine-tuning of Lewis and Brønsted sites can enable sequential transformations. Furthermore, the significance of DMSO supplementation to water for enabling sequential conversion can be verified from the results of varied aqueous-organic ratios (Fig. S9a†). As can be seen (Fig. S9b–d†), an increased water ratio from 2 : 3 to 4 : 1 to DMSO had a detrimental effect on HMF formation, *i.e.*, decreasing to 28.3% (with 47.5% selectivity), with enormous residual fructose of 16.4%, resulting in a decreased TON up to 0.0210 s^{-1} (Tables S5–S7†). This implies that water is a preferred medium for glucose isomerization.[47] On the other hand, the large volume of water (1 : 4 ratio of W/DMSO) has induced HMF rehydration under the prevailing conditions, achieving 5–8% LA and 3–5% FA (Table S6†), which is close to the productivity of a plain water medium (Table S2†). The study of the effect of reaction time disclosed that a prolonged reaction is optimum for maximum productivity, *i.e.*, 180 min to yield 78.6% HMF. According to the literature, a sequential conversion pathway is appropriate to achieve

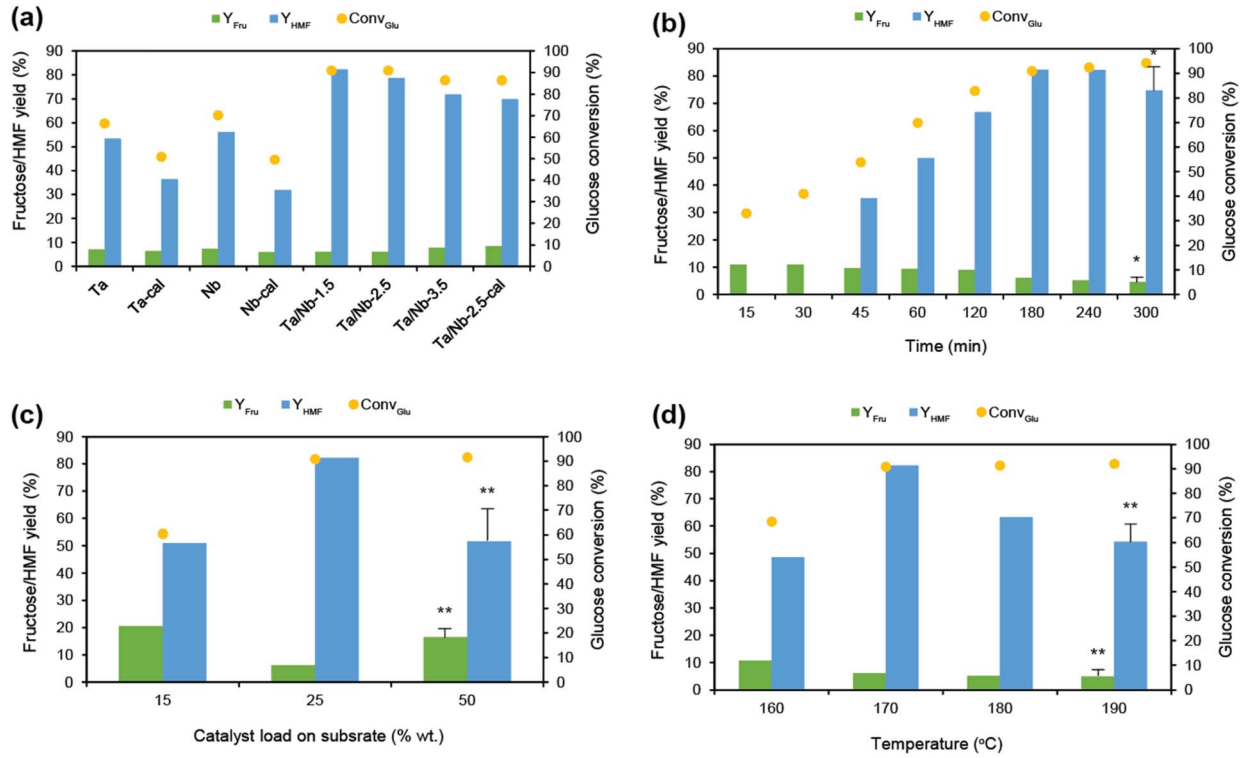

Fig. 5 (a) Effectiveness of the catalyst in glucose decomposition to HMF in an aqueous-organic solvent medium (1 : 4 vol. ratio W/DMSO) at 170 °C and 25% wt catalyst load after 3 h; (b) time optimization of glucose decomposition to HMF in a 1 : 4 vol. ratio W/DMSO medium at 170 °C and 25% wt catalyst load; (c) effect of catalyst load on glucose at 170 °C up to 3 h; (d) effect of temperature on glucose decomposition to HMF in 1 : 4 vol. ratio W/DMSO medium at 25% wt catalyst load after 3 h. Y-yield and conv-conversion. The error bar represents the standard error. The asterisk marks (* and **) denote the mean data significance and non-significance through ANOVA analysis at $\alpha = 0.05$.

a maximum HMF yield within 120–180 min.[13] The glucose conversion to HMF necessitates an extended reaction time of up to 10–15 hours.[11,48] In this study, the maximum HMF formation (78.6%) was obtained after 180 min (Fig. 5b and Table S4†).

Following this, the optimization of catalyst loading and temperature was performed under similar conditions. A lower catalyst load on the substrate struggled to enable sequential conversions, resulting in only a 47.3% yield of HMF but with 20.5% residual fructose (Fig. 5c). On the other hand, an excessive catalyst loading, which provides an excess of active sites (Lewis/Brønsted acid), led to reduced productivity (48.0% HMF yield and 52.4% selectivity), with a TON of 0.0232 s^{-1} (Table S8†). Typically, a high-severity condition can induce side reactions by consuming the formed fructose and HMF due to their reactive characteristics. This resulted in the formation of 9.8% LA and 6.3% FA, with a nearly 20% reduction in fructose concentration, along with the formation of several non-traceable degradation products. Therefore, a 1 : 4 ratio of catalyst load (Ta/Nb-2.5) to glucose can be considered optimum. A similar trend of HMF production was observed on varying the temperature (Fig. 5d and S10†). Lower temperatures (<170 °C) were found to be ineffective, resulting in only a 44.9% HMF yield but with 65.6% selectivity (Tables S9 and S10†). Conversely, higher temperatures (180–190 °C) had an adverse effect on the reaction (Tables S11 and S12†), reducing the yield and selectivity proportionately (as low as 50.1% HMF) and promoting the formation of maximum byproducts (13.3% LA and 8.5% FA). At 170 °C, maximum HMF productivity was achieved (Fig. 5d). However, under all elevated conditions, the residual fructose concentration remained at an average of 8.3%. This indicates the proficiency of the catalyst to continuously supply fructose even beyond the upper limit of equilibrium, *i.e.*, >80%, assuming complete conversion of fructose into HMF is achieved, regardless of the reaction severity. This considerable residual fructose recovery can be interpreted as its preference for equilibrium with glucose in a water-supplemented medium.[47] The results of glucose isomerization to fructose over Ta/Nb-2.5 at 120 °C (which is favorable for the reaction) establish the thermodynamic equilibrium characteristics by yielding 10.1% fructose in water (Fig. S11†) and 17.7% in binary solvent media (Fig. S12†). In a typical reaction, DMSO is helpful; it is attributed to its acidic characteristics under elevated conditions.[13,49] Due to this, a 14% HMF accounts for it in an overall product synthesis. Thus, the results substantiate the significance of the combination of Lewis and Brønsted acidic sites. The results of calcined Ta/Nb-2.5 disclosed the effect of catalyst porosity, affording only 69.9% HMF, which is relatively 11% lower than the productivity of Ta/Nb-2.5 without calcination (Fig. 5a). From these, the acidic strength, along with the structural characteristics, is crucial for effective sugar catalysis.

Impact of Lewis/Brønsted acidic sites on fructose dehydration to HMF

In a typical reaction, fructose's role is significant because it serves as a potential precursor for HMF production. From the results of glucose conversion to HMF, the ability of the catalyst to offer favorable Lewis acid sites can somewhat confirm its role in promoting the initial sugar conversion. However, since these sites are not effective in fructose dehydration, it is presumed that the prevalent Brønsted acid sites govern the secondary transformation.[17] But the latter can influence tandem catalysis of fructose to glucose (*via* a reverse reaction due to an isomer) and HMF (*via* forward dehydration). Therefore, we investigated the potential of Ta/Nb-2.5 in fructose dehydration. For this purpose, we considered all the as-synthesized catalysts, including pristine and mixed metal oxides with and without calcination. Since water has been reported as unsuitable for a dehydration reaction,[49] the catalysts were only able to form HMF to a limited extent (46%) under similar operating conditions (Fig. S13†). Among all the catalysts tested, Ta/Nb-2.5 exhibited superior performance (TON = 0.0201 s^{-1}) (Table S14†), attributed to its higher Brønsted acid characteristics (as high as 75.8%). However, it allowed for nearly 5–7% glucose formation *via* a tandem reaction in a water medium (Fig. S14 and Table S15†), with nominal co-formations (<1% LA and FA yields). In contrast, in a binary solvent medium (1 : 4 vol. ratio of W/DMSO), all catalysts showed an excellent HMF productivity, achieving a maximum HMF concentration of 92.3% and selectivity of 92.3% (Fig. 6a), with the Ta/Nb-2.5 catalyst ranking first with a TON of 0.0451 s^{-1} (Table S16†). Using a proficient catalyst, we conducted time and catalyst loading optimization studies, determining that a 3 h reaction was found to be optimum at a 25% load (Fig. 6b–c, Tables S17 and S18†). Similarly, increasing the temperature from 160 °C to 170 °C significantly impacted the conversion, providing 92.3% HMF yield and selectivity (Tables S17 & S19†). However, higher temperatures (>170 °C) were detrimental (Fig. 6d), leading to side formations and a higher LA yield (as high as 23.6%) through the degradation of HMF (resulting in a decrease to 63.5%) (Fig. S15, Tables S20 and S21†), because HMF is unstable under high-temperature conditions in an acidic medium.[50] This supports the assumption that Brønsted acidic sites have a higher contribution to the synthesis of HMF.

Plausible reaction mechanism of Ta_2O_5/Nb_2O_5 induced glucose conversion to HMF

From the sugar(s) dehydration results, the activity of both Lewis and Brønsted acid sites offered by the Ta_2O_5/Nb_2O_5 composite is significant in the stepwise conversion of glucose into HMF. Therefore, a plausible reaction mechanism can be proposed by assuming glucose isomerization to fructose over Lewis acid sites and fructose dehydration to HMF over Brønsted acid sites.[17,47] Notably, both metal oxides can offer both acidic sites;

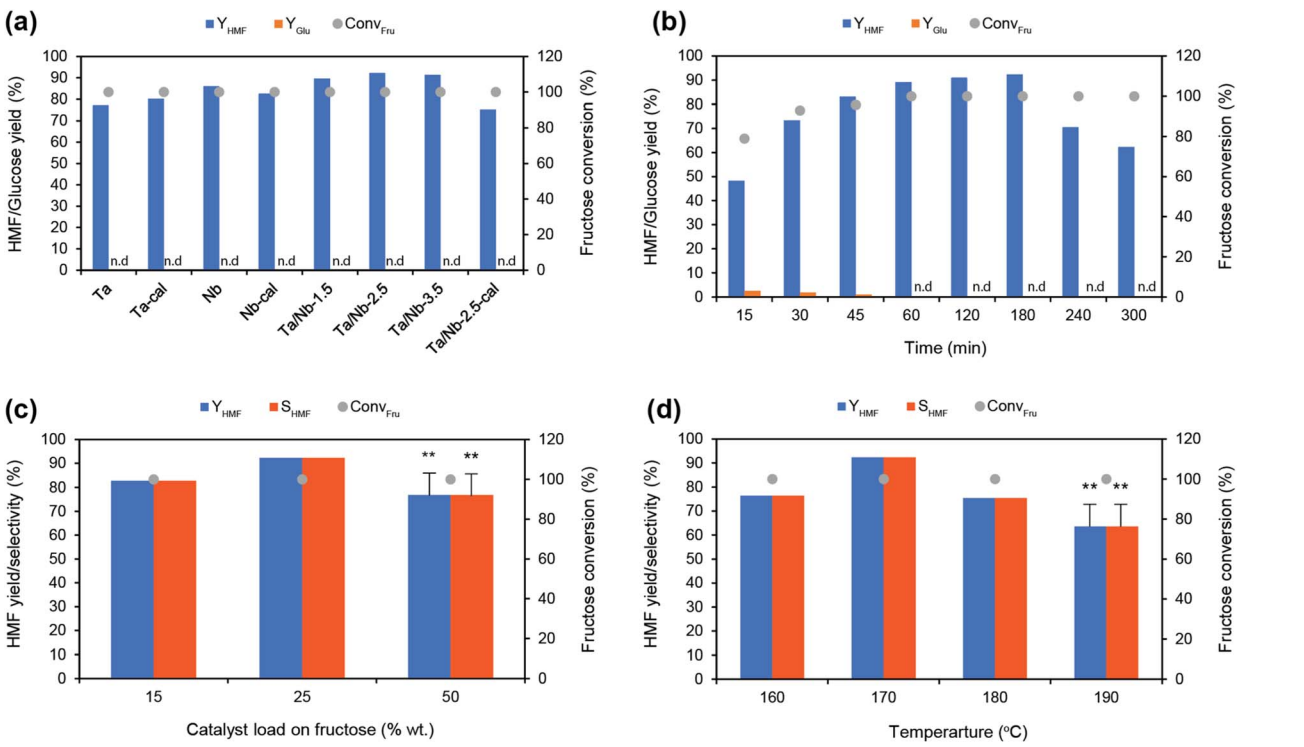

Fig. 6 (a) Effectiveness of the catalyst in fructose decomposition to HMF in an aqueous-organic solvent medium (1 : 4 vol. ratio W/DMSO) at 170 °C and 25% wt catalyst load after 3 h; (b) time optimization of fructose decomposition to HMF in a 1 : 4 vol. ratio W/DMSO medium at 170 °C and 25% wt catalyst load; (c) effect of catalyst load on fructose at 170 °C up to 3 h; (d) effect of temperature on fructose decomposition to HMF in a 1 : 4 vol. ratio W/DMSO medium at 25% wt catalyst load after 3 h. Y-yield, S-selectivity and conv-conversion. N. D.-not detected. The error bar represents the standard error. The asterisk marks (* and **) denote the mean data significance and non-significance through ANOVA analysis at $\alpha = 0.05$.

therefore, it is assumed that both of them are involved in the reaction, as proposed in Scheme 1. Thus, either or both Ta and Nb metal species can initiate the reaction through interaction with the oxygens of the carbonyl and C2 hydroxyl groups of acyclic glucose, yielding complex 1, which can undergo deprotonation at the C2 hydroxyl group. This can trigger a 1,2-hydride shift through the formation of a complex HT, where Lewis acidity can play a vital role in transferring hydrogen from C2 to C1, resulting in the formation of a carbonyl ketone at the C2 position (complex 2). The resulting compound can be easily hydrolyzed by the surrounding water molecules, yielding fructose and releasing the catalyst into the medium. Under the prevailing conditions, fructose tends to undergo reverse isomerization to yield glucose. This can be controlled by the active Brønsted acidic sites, which immediately consume the fructose to form HMF. Therefore, only a minor amount of glucose is

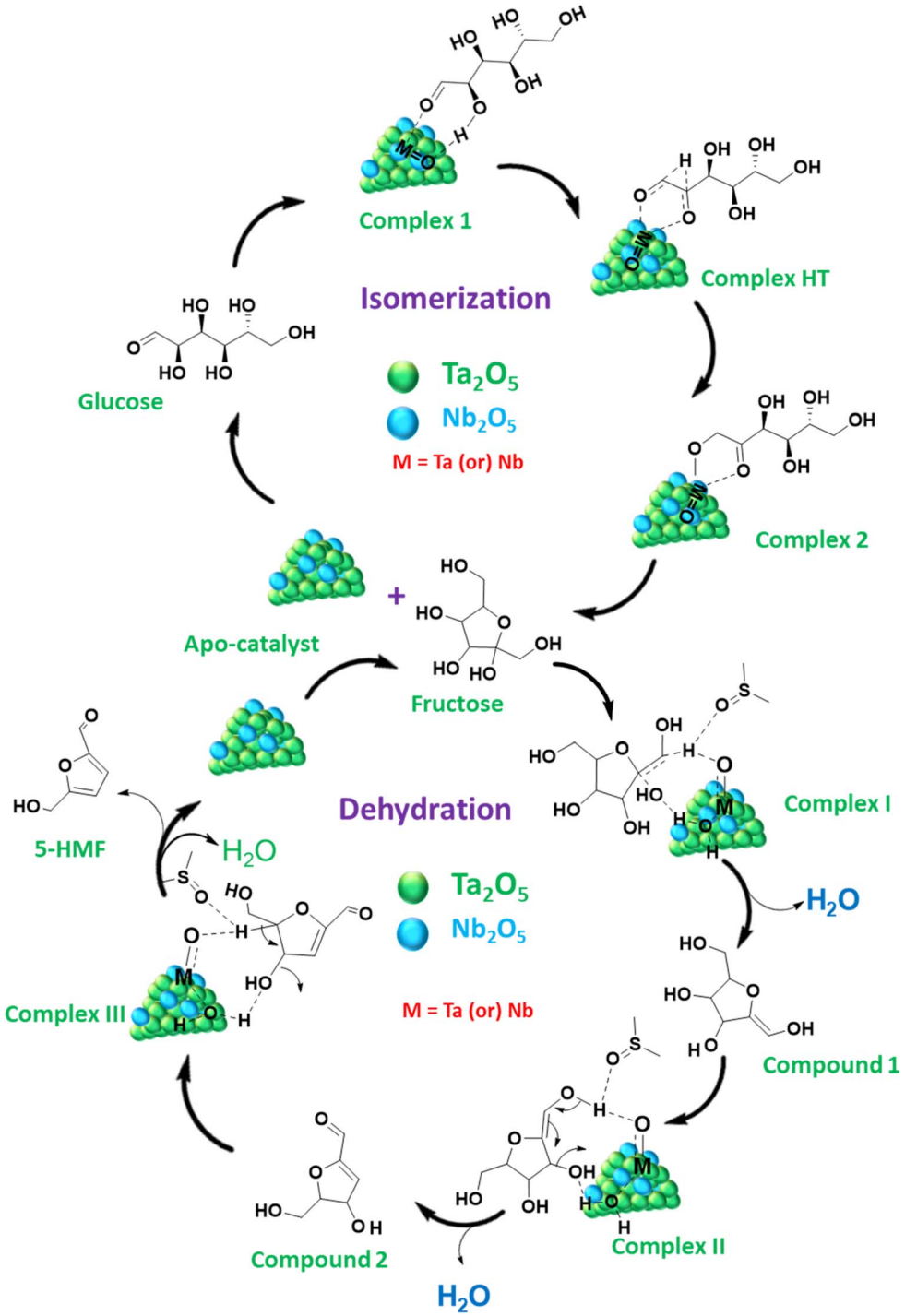

Scheme 1 Proposed reaction mechanism of glucose to HMF *via* fructose formation over the Ta_2O_5/Nb_2O_5 nanocomposite exhibiting both Lewis and Brønsted acid sites in a DMSO medium.

formed, consistent with the glucose/fructose hydration results (Fig. S10 & S15†). According to the analytical characterization, Nb_2O_5 offers a relatively higher number of Brønsted acid sites (Table 1), resulting in Ta/Nb-2.5 exhibiting the maximum number of strong acid sites. Thus, its contribution can be considered comparatively higher in the subsequent conversion of fructose. If so, the dehydration reaction can be initiated through the interaction of the C1 hydrogen with the oxygen of Nb_2O_5 (Scheme 1). With the influence of the catalytic sites, the oxygen of the C2 hydroxyl group can also interact with the Nb species, causing the release of a water molecule *via* dehydration (first dehydration), resulting in compound 1. This can be transformed into complex II, which can then undergo a second dehydration to form compound 2 by removing hydrogen from the hydroxyl groups linked to the C1 and C2 carbons.

Eventually, this can lead to the formation of complex III, which can undergo the elimination of another water molecule (third dehydration) between the C4 and C5 carbons *via* a similar interaction mechanism between the complex molecule and the catalyst. This results in the formation of HMF and an apo catalyst, which can be active for recycling.

Kinetic mechanism and energetics of glucose/fructose conversion to HMF

Thus, the results validated the sequential transformation of glucose into HMF *via* fructose intermediate formation under acidic conditions. In order to gain insights into the reaction competitiveness, which leads to significant residual fructose, a typical kinetic model was used. For this purpose, we employed the kinetic model developed by Zhang *et al.*,[21] which includes the rate kinetics of glucose and fructose decompositions. To simplify the determination of rate constants, we mainly neglected the formation of soluble/insoluble humin, LA and FA, and polymeric byproducts. Additionally, we assumed that the reversibility of fructose to glucose is negligible. Furthermore, we assumed that glucose dehydration follows second-order rate kinetics, while fructose dehydration to HMF and humin follows a first-order rate law. According to Scheme 2, the differential form of the rate equations for the degradation reactions of the reactant and product can be derived as:

$$\frac{d[Glu]}{dt} = -k_G[Glu]^2 \quad (1)$$

$$\frac{d[Fru]}{dt} = k_G[Glu]^2 - (k_1 + k_2)[Fru] \quad (2)$$

$$\frac{d[HMF]}{dt} = k_1[Fru] \quad (3)$$

Based on the low fructose residual concentration, a steady-state approximation can be applied to simplify the model. Therefore, eqn (2) can be reduced and rearranged to obtain a final form of eqn (3) represented as eqn (4):

$$\frac{d[HMF]}{dt} = \frac{k_1 k_G}{k_1 + k_2}\left(\frac{[Glu]_0}{1 + k_G[Glu]_0 t}\right)^2 \quad (4)$$

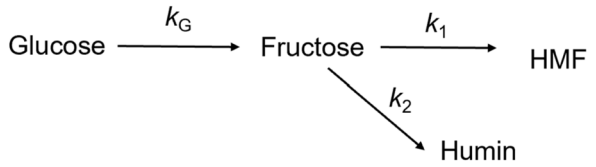

Scheme 2 Kinetic scheme of glucose conversion to HMF *via* fructose intermediate formation.

Fig. 7a displays a linear fit of glucose degradation ($1/[Glu]_t - 1/[Glu]_0$) with respect to time, affirming its second-order degradation with a k_G of 2.4×10^{-2} L mol^{-1} s^{-1} at the optimum temperature, consistent with the assumption. Moreover, an increasing magnitude of the rate constant from 1.0×10^{-2} to 4.3×10^{-2} L mol^{-1} s^{-1} with respect to temperature (160–190 °C) affirms that temperature accelerates the degradation (Fig. S16†), leading to the formation of fructose, which can be instantly transformed into HMF over the Brønsted acidic sites. For clarity, the formation of FA and humin using glucose was not considered. On determining the rate kinetics of fructose degradation, it exhibited a first-order degradation by establishing a linear trend between $\ln[Fru]_t/[Fru]_0$ and time, with a k_F of 1.3×10^{-3} s^{-1} under optimum conditions (Fig.-S17a†). Fig. S17a† also shows the impact of temperature with a variation of $k_F = 9.6 \times 10^{-4}$–1.5×10^{-3} s^{-1} for the 160–190 °C range (a correlation plot can be seen in Fig. S18†). With these two different orders of reactions, it may be difficult to ascertain the reaction competitiveness. Evidently, the temperature had a significant impact on the overall kinetics, enabling up to 100 times faster sugar decomposition. Due to the reactive characteristics of fructose, it can undergo a two-way degradation under stringent conditions: one leads to yielding an ultimate HMF (reaction (1)) and another to forming an unwanted humin byproduct (reaction (2)). The linear fashion of these reaction kinetics with respect to time confirms their first-order product formation. At the optimum temperature, k_{HMF} was determined to be 8.7×10^{-4} s^{-1} (Fig. S17b†) and k_{Hum} to be 4.7×10^{-5} s^{-1} (Fig. S19†); this clearly indicates the preferential fructose decomposition to HMF *via* dehydration rather compared to the other. At the same time, HMF can undergo unwanted degradations at elevated temperatures, including cross-polymerization between HMF and the intermediates, and humin. Due to this, a slower rate of formation was observed at 190 °C (relatively ~20% slower than the optimum rate). This can be seen reflected in faster humin formation, *i.e.*, relatively 18% at 190 °C (Fig. S19†). Furthermore, we determined the temperature-dependent characteristics of the reaction steps by applying the principles of the Arrhenius theory (eqn (S5)†).[51] The plots of $\ln k_G$ and $\ln k_F$ *vs.* temperature established a linear correlation (Fig. 7b and S17c†), suggesting the temperature-dependent kinetics of glucose and fructose, with activation energies E_a of 79.7 kJ mol^{-1} and 23.5 kJ mol^{-1}, respectively. This discloses that glucose decomposition is highly energy-intensive, requiring three times more energy to overcome the energy barrier developed by the *in situ* conversions, specifically glucose to fructose isomerization, which is consistent with the literature.[52,53] Reactions (1) & (2) determined the E_a to be

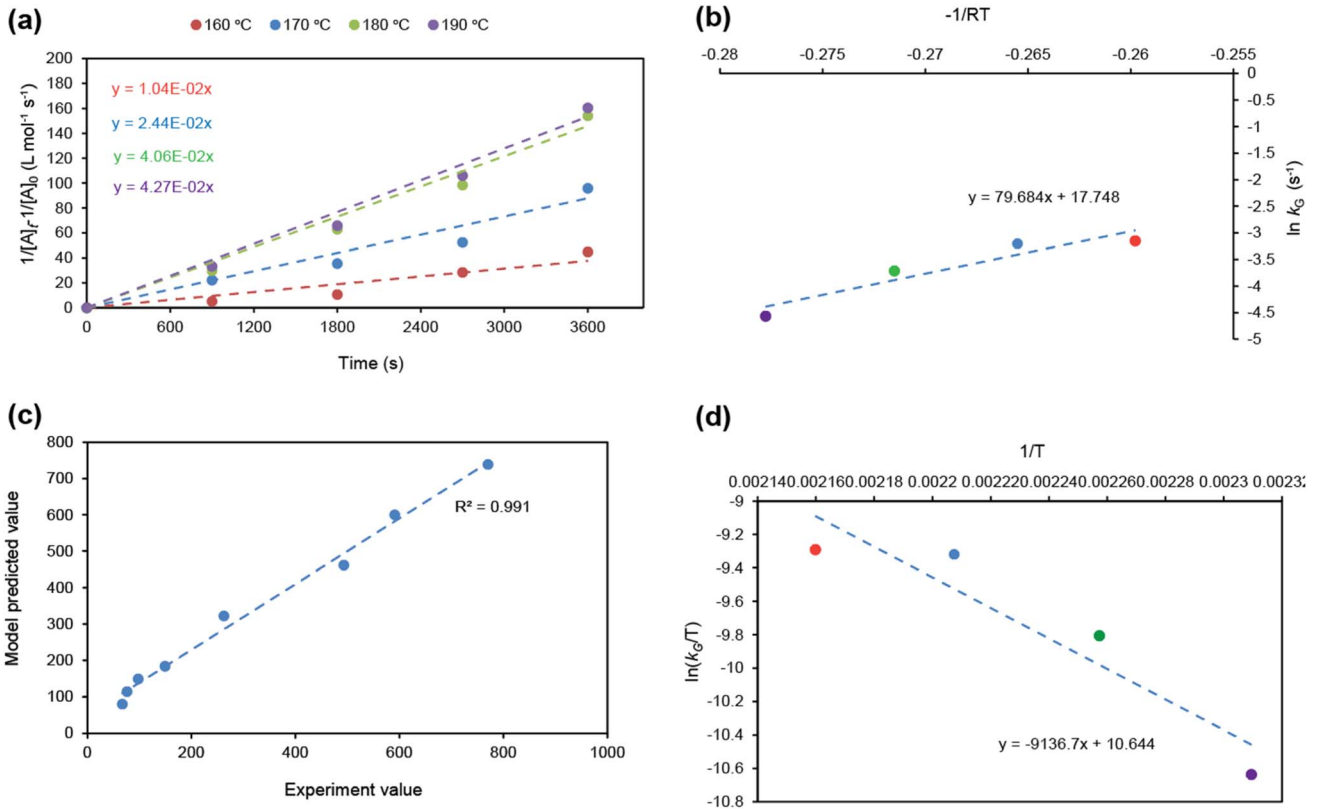

Fig. 7 (a) Second-order kinetics of glucose decomposition over the Ta/Nb-2.5 catalyst in 1 : 4 vol. ratio W/DMSO under different temperature conditions (160–190 °C) at 25% wt catalyst load up to 5 h; (b) Arrhenius plot of rate kinetics of glucose decomposition over the Ta/Nb-2.5 catalyst in 1 : 4 vol. ratio W/DMSO under different temperature conditions (160–190 °C); (c) correlation plot of experimental *vs.* predicted values of glucose degradation over the Ta/Nb-2.5 catalyst in 1 : 4 vol. ratio W/DMSO at 170 °C; (d) Eyring plot of rate kinetics of glucose decomposition over the Ta/Nb-2.5 catalyst in 1 : 4 vol. ratio W/DMSO under different temperature conditions (160–190 °C).

12.2 kJ mol^{-1} and 16.9 kJ mol^{-1}, respectively (Fig. S17c†), revealing fructose's reactivity attributes. Moreover, the model had a fair prediction of the decaying glucose concentration and HMF formation, as shown in Fig. 7c and S20,† respectively.

Additionally, we calculated the thermodynamic parameters to determine the feasibility of the reaction by employing the transition state Eyring theory (eqn (5)).[54]

$$\ln\left(\frac{k}{T}\right) = \ln\left(\frac{k_B}{h}\right) + \frac{\Delta S^{\neq}}{R} - \frac{\Delta H^{\neq}}{RT} \quad (5)$$

where k is the rate constant (s^{-1}); T is the temperature (K); $\Delta H^{\#}$ is the activation enthalpy; $\Delta S^{\#}$ is the activation entropy; k_B is the Boltzmann constant (1.381×10^{-23} J K^{-1}); h is Planck's constant (6.626×10^{-34} J s^{-1}) and R is the universal gas constant (9.314 J mol^{-1} K^{-1}). The $\Delta H^{\#}$ values for the glucose and fructose conversions were estimated to be 75.9 kJ mol^{-1} (Fig. 6d) and 19.8 kJ mol^{-1} (Fig. S17d†), respectively. The positive values indicate the endothermic nature of the reactions, meaning that external energy is necessary to induce substrate–catalyst complexation. However, the fructose conversion has an estimated 3.5 times lower enthalpy of activation, suggesting that less energy is needed to activate the fructose–catalyst complex formation. The higher energy input required for the conversion of glucose into HMF can be attributed to the formation of a transition state from a relatively stable 6-membered ring of glucose. The typical $\Delta S^{\#}$ values determine the randomness of a reaction, with higher positive values defined as highly disordered (or a spontaneous reaction). Unfortunately, both glucose and fructose conversions have estimated negative values of −109.0 J mol^{-1} K^{-1} and −259.6 J mol^{-1} K^{-1}, respectively. This decrease in entropy during these transformations is likely caused by the interference of a number of unwanted molecules (including humin) in the formation of the transition state molecules.[54] Of these, fructose decomposition was established to be a highly disordered system due to its enhanced degradation to levulinic acid, formic acid, *etc.* Similarly, reactions (1) & (2) have estimated slightly higher $\Delta S^{\#}$ values of −288.7 J mol^{-1} K^{-1} and −300.9 J mol^{-1} K^{-1}, respectively (Fig. S17d†), representing energy-intensive conversions, which is approximately 3 times higher than that of glucose decomposition under the prevailing conditions. Using these data, the reaction activation free energy (ΔG°) can be calculated for the glucose and fructose decompositions (using eqn (S6)†).[54] The former conversion has an estimated ΔG° of 124.2 kJ mol^{-1}, while that of the latter is calculated to be 132.5 kJ mol^{-1}, establishing a comparable energy involvement. These positive values suggest the non-spontaneous characteristics of the reactions, which is consistent with literature reports.[51,54] Thus, the results suggest that the conversion of glucose into HMF is energetically less viable compared to fructose transformation, resulting in only 90.9% glucose conversion

under optimum conditions. However, elevated temperatures can influence side reactions involving fructose as an intermediate. Although fructose conversion is demonstrated to be an easier step, achieving 100% conversion within 60 min, significant residual fructose recovery can be interpreted as its equilibrium characteristics with glucose.[47]

Recycling efficiency of the catalyst

The recycling efficiency of the Ta/Nb-2.5 catalyst was evaluated under optimum conditions using glucose/fructose. The results confirmed its robustness by achieving a similar HMF productivity for up to 5 reuses (Fig. S21–S22 and Table S22†), with a hardly 1–4% difference. While verifying the structural characteristics of the recycled catalyst after six runs (including the fresh run) *via* FTIR and XRD analyses, it can be observed that it retains the original configuration (Fig. S23a and b†). Furthermore, the EDX results reveal the catalyst's composition to be 16.6% Nb, 29.2% Ta, and 54.2% O (Fig. S24†), closely matching the results of the fresh ones. However, a decrease in HMF selectivity is likely caused by the effect of impurities deposited on the catalyst's surface.[55] The textural and surface measurements determined the characteristics, with a total pore volume of 0.1168 $cm^3 g^{-1}$, an average pore radius of 1.39 nm, and a surface area of 181.448 $m^2 g^{-1}$. This observed reduction in pore radius (approximately 3%), resulting in an increased surface area (approximately 26% more than that of fresh Ta/Nb-2.5), can be correlated with pore blockage caused by humin deposition. However, nearly the same number of acidic sites, approximately 0.635 mmol g^{-1}, was measured through a TPD method (Fig. S25†). The carbon balance, calculated by including unconverted glucose, formed fructose, HMF, formic acid, and levulinic acid, showed a value of 98.62% under optimum conditions. When comparing the results with the literature employing metal oxide catalysts, the Ta_2O_5/Nb_2O_5 composite achieved a nearly 20% to 3-fold higher HMF productivity (as shown in Table S23†).

Conclusions

Herein, we demonstrate the design and development of a solid acid catalyst that offers both Lewis and Brønsted acid sites for its application in effectively converting glucose into HMF. The Ta_2O_5/Nb_2O_5 composite, comprising 25% Nb_2O_5, is able to provide a balanced Lewis/Brønsted acid site distribution, resulting in a stepwise conversion of glucose isomerization to fructose and fructose dehydration to HMF. This results in a maximum HMF yield of 78.6% and a selectivity of 86.5% under modest reaction conditions. Furthermore, the composite catalyst exhibits robustness for recycling for up to 5 runs without any compromise in HMF productivity and structural features. Thus, the metal oxide-based catalytic setup represents an eco-friendly and sustainable method for bioenergy development.

Conflicts of interest

The authors declare that they have no competing interests.

Author contributions

Sangeeta Mahala and Sasikumar Elumalai: conceptualization, methodology, investigation, original draft preparation. Sangeeta Mahala, Senthil Murugan Arumugam, Ravi Kumar Kunchala and Bhawana Devi: data analysis, writing – reviewing and editing. Sasikumar Elumalai: visualization, supervision, funding, writing – reviewing and editing.

Acknowledgements

Sangeeta Mahala thanks the Department of Biotechnology (DBT), New Delhi, for the financial support through the Senior Research Fellowship (Flagship Project Grant No. BT/CIAB-Flagship/2018). The authors thank the Department of Biotechnology (DBT), New Delhi, for their consistent financial support and laboratory cum instrument facilities.

References

1 K. Alper, K. Tekin, S. Karagöz and A. J. Ragauskas, Sustainable energy and fuels from biomass: a review focusing on hydrothermal biomass processing, *Sustainable Energy Fuels*, 2020, **4**(9), 4390–4414, DOI: 10.1039/d0se00784f.

2 A. Bušić, N. Marđetko, S. Kundas, G. Morzak, H. Belskaya, M. Ivančić Šantek, D. Komes, S. Novak and B. Šantek, Bioethanol Production from Renewable Raw Materials and Its Separation and Purification: A Review, *Food Technol. Biotechnol.*, 2018, **56**(3), 289–311, DOI: 10.17113/ftb.56.03.18.5546.

3 X. Tong, Y. Ma and Y. Li, Biomass into chemicals: conversion of sugars to furan derivatives by catalytic processes, *Appl. Catal., A*, 2010, **385**(1), 1–13, DOI: 10.1016/j.apcata.2010.06.049.

4 S. Kumar, V. Ahluwalia, P. Kundu, R. S. Sangwan, S. K. Kansal, T. M. Runge and S. Elumalai, Improved levulinic acid production from agri-residue biomass in biphasic solvent system through synergistic catalytic effect of acid and products, *Bioresour. Technol.*, 2018, **251**, 143–150.

5 J. B. Binder and R. T. Raines, Simple Chemical Transformation of Lignocellulosic Biomass into Furans for Fuels and Chemicals, *J. Am. Chem. Soc.*, 2009, **131**(5), 1979–1985, DOI: 10.1021/ja808537j.

6 A. A. Rosatella, S. P. Simeonov, R. F. M. Frade and C. A. M. Afonso, 5-Hydroxymethylfurfural (HMF) as a building block platform: biological properties, synthesis and synthetic applications, *Green Chem.*, 2011, **13**(4), 754–793, DOI: 10.1039/c0gc00401d.

7 W. Guo, Z. Zhang, J. Hacking, H. J. Heeres and J. Yue, Selective fructose dehydration to 5-hydroxymethylfurfural from a fructose-glucose mixture over a sulfuric acid catalyst in a biphasic system: experimental study and kinetic modelling, *Chem. Eng. J.*, 2021, **409**, 128182, DOI: 10.1016/j.cej.2020.128182.

8 Y. Qu, Y. Zhao, S. Xiong, C. Wang, S. Wang, L. Zhu and L. Ma, Conversion of Glucose into 5-Hydroxymethylfurfural and

Levulinic Acid Catalyzed by SO_4^{2-}/ZrO_2 in a Biphasic Solvent System, *Energy Fuels*, 2020, **34**(9), 11041–11049, DOI: 10.1021/acs.energyfuels.0c01823.

9 B. Agarwal, K. Kailasam, R. S. Sangwan and S. Elumalai, Traversing the history of solid catalysts for heterogeneous synthesis of 5-hydroxymethylfurfural from carbohydrate sugars: a review, *Renewable Sustainable Energy Rev.*, 2018, **82**, 2408–2425, DOI: 10.1016/j.rser.2017.08.088.

10 Y. Zhao, K. Lu, H. Xu, L. Zhu and S. Wang, A critical review of recent advances in the production of furfural and 5-hydroxymethylfurfural from lignocellulosic biomass through homogeneous catalytic hydrothermal conversion, *Renewable Sustainable Energy Rev.*, 2021, **139**, 110706, DOI: 10.1016/j.rser.2021.110706.

11 R. Sharma, A. Selim, B. Devi, S. M. Arumugam, S. Sartaliya, S. Elumalai and G. Jayamurugan, Realizing direct conversion of glucose to furfurals with tunable selectivity utilizing a carbon dot catalyst with dual acids controlled by a biphasic medium, *Biomass Convers. Biorefin.*, 2022, DOI: 10.1007/s13399-022-03182-w.

12 D. Gupta, E. Ahmad, K. K. Pant and B. Saha, Efficient utilization of potash alum as a green catalyst for production of furfural, 5-hydroxymethylfurfural and levulinic acid from mono-sugars, *RSC Adv.*, 2017, **7**(67), 41973–41979, DOI: 10.1039/c7ra07147g.

13 S. Mahala, S. M. Arumugam, S. Kumar, D. Singh, S. Sharma, B. Devi, S. K. Yadav and S. Elumalai, Sn Doping on Ta_2O_5 Facilitates Glucose Isomerization for Enriched 5-Hydroxymethylfurfural Production and its True Response Prediction using a Neural Network Model, *ChemCatChem*, 2021, **13**(22), 4787–4798, DOI: 10.1002/cctc.202101046.

14 Y. Román-Leshkov, M. Moliner, J. A. Labinger and M. E. Davis, Mechanism of Glucose Isomerization Using a Solid Lewis Acid Catalyst in Water, *Angew. Chem., Int. Ed.*, 2010, **49**(47), 8954–8957, DOI: 10.1002/anie.201004689.

15 P. Körner, D. Jung and A. Kruse, The effect of different Brønsted acids on the hydrothermal conversion of fructose to HMF, *Green Chem.*, 2018, **20**(10), 2231–2241, DOI: 10.1039/c8gc00435h.

16 I. Jiménez-Morales, M. Moreno-Recio, J. Santamaría-González, P. Maireles-Torres and A. Jiménez-López, Mesoporous tantalum oxide as catalyst for dehydration of glucose to 5-hydroxymethylfurfural, *Appl. Catal., B*, 2014, **154–155**, 190–196, DOI: 10.1016/j.apcatb.2014.02.024.

17 F. Yang, Q. Liu, X. Bai and Y. Du, Conversion of biomass into 5-hydroxymethylfurfural using solid acid catalyst, *Bioresour. Technol.*, 2011, **102**(3), 3424–3429, DOI: 10.1016/j.biortech.2010.10.023.

18 F. Yang, Q. Liu, M. Yue, X. Bai and Y. Du, Tantalum compounds as heterogeneous catalysts for saccharide dehydration to 5-hydroxymethylfurfural, *Chem. Commun.*, 2011, **47**(15), 4469–4471, DOI: 10.1039/c0cc05138a.

19 K. Nakajima, Y. Baba, R. Noma, M. Kitano, J. N. Kondo, S. Hayashi and M. Hara, $Nb_2O_5 \cdot nH_2O$ as a Heterogeneous Catalyst with Water-Tolerant Lewis Acid Sites, *J. Am. Chem. Soc.*, 2011, **133**(12), 4224–4227, DOI: 10.1021/ja110482r.

20 G. Orsini and V. Tricoli, Facile nonhydrolytic sol–gel route to mesoporous mixed-conducting tungsten oxide, *J. Mater. Chem.*, 2011, **21**(38), 14530–14542, DOI: 10.1039/c1jm10777a.

21 J. Zhang, Y. Cao, H. Li and X. Ma, Kinetic studies on chromium-catalyzed conversion of glucose into 5-hydroxymethylfurfural in alkylimidazolium chloride ionic liquid, *Chem. Eng. J.*, 2014, **237**, 55–61, DOI: 10.1016/j.cej.2013.10.007.

22 J. J. Wiesfeld, R. Gaquere and E. J. M. Hensen, Mesoporous Doped Tungsten Oxide for Glucose Dehydration to 5-Hydroxymethylfurfural, *ACS Sustain. Chem. Eng.*, 2019, **7**(8), 7552–7562, DOI: 10.1021/acssuschemeng.8b05684.

23 D. Rathnayake, I. Perera, A. Shirazi-Amin, P. Kerns, S. Dissanayake and S. L. Suib, Mesoporous Crystalline Niobium Oxide with a High Surface Area: A Solid Acid Catalyst for Alkyne Hydration, *ACS Appl. Mater. Interfaces*, 2020, **12**(42), 47389–47396, DOI: 10.1021/acsami.0c10757.

24 S. Li, Q. Xu, E. Uchaker, X. Cao and G. Cao, Comparison of amorphous, pseudohexagonal and orthorhombic Nb_2O_5 for high-rate lithium ion insertion, *CrystEngComm*, 2016, **18**(14), 2532–2540, DOI: 10.1039/c5ce02069g.

25 E. L. S. Ngee, Y. Gao, X. Chen, T. M. Lee, Z. Hu, D. Zhao and N. Yan, Sulfated Mesoporous Niobium Oxide Catalyzed 5-Hydroxymethylfurfural Formation from Sugars, *Ind. Eng. Chem. Res.*, 2014, **53**(37), 14225–14233, DOI: 10.1021/ie501980t.

26 N. C. Stephenson and R. S. Roth, The crystal structure of the high temperature form of Ta_2O_5, *J. Solid State Chem.*, 1971, **3**(2), 145–153, DOI: 10.1016/0022-4596(71)90018-1.

27 R. Abdul Rani, A. S. Zoolfakar, N. S. Khairir, M. H. Mamat, S. Alrokayan, H. A. Khan and M. R. Mahmood, Hydrothermal synthesis of nanomoss Nb_2O_5 films and their ultraviolet photodetection performance, *J. Mater. Sci.: Mater. Electron.*, 2018, **29**(19), 16765–16774, DOI: 10.1007/s10854-018-9770-0.

28 S. Ambreen, N. D. Pandey, P. Mayer and A. Pandey, Characterization and photocatalytic study of tantalum oxide nanoparticles prepared by the hydrolysis of tantalum oxo-ethoxide $Ta_8(\mu_3\text{-}O)_2(\mu\text{-}O)_8(\mu\text{-}OEt)_6(OEt)_{14}$, *Beilstein J. Nanotechnol.*, 2014, **5**, 1082–1090, DOI: 10.3762/bjnano.5.121.

29 A. K. Kulkarni, C. S. Praveen, Y. A. Sethi, R. P. Panmand, S. S. Arbuj, S. D. Naik, A. V. Ghule and B. B. Kale, Nanostructured N-doped orthorhombic Nb_2O_5 as an efficient stable photocatalyst for hydrogen generation under visible light, *Dalton Trans.*, 2017, **46**(43), 14859–14868, DOI: 10.1039/c7dt02611k.

30 J. Yan, G. Wu, N. Guan and L. Li, Nb_2O_5/TiO_2 heterojunctions: synthesis strategy and photocatalytic activity, *Appl. Catal., B*, 2014, **152–153**, 280–288, DOI: 10.1016/j.apcatb.2014.01.049.

31 X. Yu, W. Li, Z. Li, J. Liu and P. Hu, Defect engineered Ta_2O_5 nanorod: one-pot synthesis, visible-light driven hydrogen generation and mechanism, *Appl. Catal., B*, 2017, **217**, 48–56, DOI: 10.1016/j.apcatb.2017.05.024.

32 A. M. Huerta-Flores, F. Ruiz-Zepeda, C. Eyovge, J. P. Winczewski, M. Vandichel, M. Gaberšček, N. D. Boscher, H. J. G. E. Gardeniers, L. M. Torres-Martínez and A. Susarrey-Arce, Enhanced Photocatalytic Hydrogen Evolution from Water Splitting on $Ta_2O_5/SrZrO_3$ Heterostructures Decorated with Cu_xO/RuO_2 Cocatalysts, *ACS Appl. Mater. Interfaces*, 2022, **14**(28), 31767–31781, DOI: **10.1021/acsami.2c02520**.

33 H. Yan, Y. Xie, Y. Jiao, A. Wu, C. Tian, X. Zhang, L. Wang and H. Fu, Holey Reduced Graphene Oxide Coupled with an Mo_2N–Mo_2C Heterojunction for Efficient Hydrogen Evolution, *Adv. Mater.*, 2018, **30**(2), 1704156, DOI: **10.1002/adma.201704156**.

34 S. T. Rajan, J. Senthilnathan and A. Arockiarajan, Sputter-coated N-enriched mixed metal oxides (Ta_2O_5-Nb_2O_5-N) composite: a resilient solar driven photocatalyst for water purification, *J. Hazard. Mater.*, 2023, **452**, 131283, DOI: **10.1016/j.jhazmat.2023.131283**.

35 R. K. Kunchala, D. Bhatt, R. Kalia, S. K. Samal, J. Yadav and B. S. Naidu, Effect of mixed-valence of manganese on water oxidation activity of $La_{1-x}Ca_xMnO_3$ ($0 \leq x \leq 1$) solid solutions, *Int. J. Hydrogen Energy*, 2023, **48**(40), 15092–15104, DOI: **10.1016/j.ijhydene.2023.01.018**.

36 R. K. Kunchala, D. Bhatt, R. Kalia and B. S. Naidu, Manifold improvement of water oxidation activity of $NaCoO_2$ by selective cation exchange, *Int. J. Hydrogen Energy*, 2023, **48**(10), 3952–3964, DOI: **10.1016/j.ijhydene.2022.10.167**.

37 K. Zhu, F. Shi, X. Zhu and W. Yang, The roles of oxygen vacancies in electrocatalytic oxygen evolution reaction, *Nano Energy*, 2020, **73**, 104761, DOI: **10.1016/j.nanoen.2020.104761**.

38 S. Venkataraj, R. Drese, C. Liesch, O. Kappertz, R. Jayavel and M. Wuttig, Temperature stability of sputtered niobium–oxide films, *J. Appl. Phys.*, 2002, **91**(8), 4863–4871, DOI: **10.1063/1.1458052**.

39 T. Ushikubo and K. Wada, Catalytic properties of hydrated tantalum oxide, *Appl. Catal.*, 1990, **67**(1), 25–38, DOI: **10.1016/S0166-9834(00)84429-2**.

40 H. T. Kreissl, M. M. J. Li, Y.-K. Peng, K. Nakagawa, T. J. N. Hooper, J. V. Hanna, A. Shepherd, T.-S. Wu, Y.-L. Soo and S. C. E. Tsang, Structural Studies of Bulk to Nanosize Niobium Oxides with Correlation to Their Acidity, *J. Am. Chem. Soc.*, 2017, **139**(36), 12670–12680, DOI: **10.1021/jacs.7b06856**.

41 W. Zhang, X. Shi, Z. Yan, Y. Shan, Y. Zhu, Y. Yu and H. He, Design of High-Performance Iron–Niobium Composite Oxide Catalysts for NH_3-SCR: Insights into the Interaction between Fe and Nb, *ACS Catal.*, 2021, **11**(15), 9825–9836, DOI: **10.1021/acscatal.1c01619**.

42 L. Chen, J. Li and M. Ge, DRIFT Study on Cerium–Tungsten/Titania Catalyst for Selective Catalytic Reduction of NO_x with NH_3, *Environ. Sci. Technol.*, 2010, **44**(24), 9590–9596, DOI: **10.1021/es102692b**.

43 S. Zhou, Z. Deng, Z. Wu, M. Xie, Y. Tian, Y. Wu, J. Liu, G. Li and Q. He, Ta_2O_5/rGO Nanocomposite Modified Electrodes for Detection of Tryptophan through Electrochemical Route, *Nanomaterials*, 2019, **9**(6), 811.

44 H. Li, Z. Xia, P. Yan and Z. C. Zhang, Production of crude 5-hydroxymethylfurfural from glucose by dual catalysts with functional promoters in low-boiling hybrid solvent, *Catal. Today*, 2022, **402**, 10–16, DOI: **10.1016/j.cattod.2022.01.017**.

45 Z. Xu, Y. Yang, P. Yan, Z. Xia, X. Liu and Z. C. Zhang, Mechanistic understanding of humin formation in the conversion of glucose and fructose to 5-hydroxymethylfurfural in [BMIM]Cl ionic liquid, *RSC Adv.*, 2020, **10**(57), 34732–34737, DOI: **10.1039/d0ra05641c**.

46 S. Pumrod, A. Kaewchada, S. Roddecha and A. Jaree, 5-HMF production from glucose using ion exchange resin and alumina as a dual catalyst in a biphasic system, *RSC Adv.*, 2020, **10**(16), 9492–9498, DOI: **10.1039/c9ra09997b**.

47 I. Delidovich and R. Palkovits, Catalytic Isomerization of Biomass-Derived Aldoses: A Review, *ChemSusChem*, 2016, **9**(6), 547–561, DOI: **10.1002/cssc.201501577**.

48 A. Selim, R. Sharma, S. M. Arumugam, S. Elumalai and G. Jayamurugan, Sulphonated Carbon Dots Synthesized Through a One-Pot, Facile and Scalable Protocol Facilitates the Preparation of Renewable Precursors Using Glucose/Levulinic Acid, *ChemistrySelect*, 2022, **7**(19), e202104448, DOI: **10.1002/slct.202104448**.

49 C. Jin, N. Xiang, X. Zhu, S. E, K. Sheng and X. Zhang, Selective 5-hydroxymethylfurfural production from cellulose formate in DMSO-H_2O media, *Appl. Catal., B*, 2021, **285**, 119799, DOI: **10.1016/j.apcatb.2020.119799**.

50 T. Tana, P. Han, A. J. Brock, X. Mao, S. Sarina, E. R. Waclawik, A. Du, S. E. Bottle and H.-Y. Zhu, Photocatalytic conversion of sugars to 5-hydroxymethylfurfural using aluminium(III) and fulvic acid, *Nat. Commun.*, 2023, **14**(1), 4609, DOI: **10.1038/s41467-023-40090-7**.

51 N. A. S. Ramli and N. A. S. Amin, Kinetic study of glucose conversion to levulinic acid over Fe/HY zeolite catalyst, *Chem. Eng. J.*, 2016, **283**, 150–159, DOI: **10.1016/j.cej.2015.07.044**.

52 Z. Ju, Y. Zhang, T. Zhao, W. Xiao and X. Yao, Mechanism of Glucose–Fructose Isomerization over Aluminum-Based Catalysts in Methanol Media, *ACS Sustain. Chem. Eng.*, 2019, **7**(17), 14962–14972, DOI: **10.1021/acssuschemeng.9b03241**.

53 H. Huang, X.-G. Meng, W.-W. Yu, L.-Y. Chen and Y.-Y. Wu, High Selective Isomerization of Glucose to Fructose Catalyzed by Amidoximed Polyacrylonitrile, *ACS Omega*, 2021, **6**(30), 19860–19866, DOI: **10.1021/acsomega.1c02577**.

54 R. Tomer and P. Biswas, Reaction kinetics study and the estimation of thermodynamic parameters for the conversion of glucose to 5-hydroxymethylfurfural (5-HMF) in a dimethyl sulfoxide (DMSO) medium in the presence of a mesoporous TiO_2 catalyst, *J. Taiwan Inst. Chem. Eng.*, 2022, **136**, 104427, DOI: **10.1016/j.jtice.2022.104427**.

55 G. Hurst, J. M. González-Carballo, L. Tosheva and S. Tedesco, Synergistic Catalytic Effect of Sulphated Zirconia—HCl System for Levulinic Acid and Solid Residue Production Using Microwave Irradiation, *Energies*, 2021, **14**(6), 1582.

